

## A Flexible Control Scheme for Single-Stage DAB AC/DC Converters

Liu, Bochen; Davari, Pooya; Blaabjerg, Frede

*Published in:*

Proceedings of the IEEE International Power Electronics and Application Conference and Exposition (PEAC 2018)

*DOI (link to publication from Publisher):*

[10.1109/PEAC.2018.8590531](https://doi.org/10.1109/PEAC.2018.8590531)

*Publication date:*

2018

*Document Version*

Accepted author manuscript, peer reviewed version

[Link to publication from Aalborg University](#)

*Citation for published version (APA):*

Liu, B., Davari, P., & Blaabjerg, F. (2018). A Flexible Control Scheme for Single-Stage DAB AC/DC Converters. In *Proceedings of the IEEE International Power Electronics and Application Conference and Exposition (PEAC 2018)* (pp. 1-6). IEEE Press. <https://doi.org/10.1109/PEAC.2018.8590531>

### General rights

Copyright and moral rights for the publications made accessible in the public portal are retained by the authors and/or other copyright owners and it is a condition of accessing publications that users recognise and abide by the legal requirements associated with these rights.

- Users may download and print one copy of any publication from the public portal for the purpose of private study or research.
- You may not further distribute the material or use it for any profit-making activity or commercial gain
- You may freely distribute the URL identifying the publication in the public portal -

### Take down policy

If you believe that this document breaches copyright please contact us at [vbn@aub.aau.dk](mailto:vbn@aub.aau.dk) providing details, and we will remove access to the work immediately and investigate your claim.

# A Flexible Control Scheme for Single-Stage DAB AC/DC Converters

Bochen Liu, Pooya Davari, Frede Blaabjerg  
Department of Energy Technology, Aalborg University  
bli@et.aau.dk, pda@et.aau.dk, fbl@et.aau.dk

**Abstract**— A flexible control method for a single-stage dual-active-bridge (DAB) based ac-dc converter is proposed. In order to avoid look-up tables and extend the achievable transfer power range, the proposed control scheme utilizes light and heavy load operation modes and adopt the suitable mode depending on the output power level. Meanwhile, unity power factor and zero-voltage switching (ZVS) can be achieved during one full-range mains cycle. Simulation results and experimental results are presented to validate the proposed method and theoretical analysis.

**Keywords**— *single-stage, DAB, ZVS, power range*

## I. INTRODUCTION

As a fundamental part of the power electronic system, ac to dc conversion or vice versa are inevitably exist as the main conversion stage of many applications. In some cases, galvanic isolation is required in consideration of safety issues or to comply with standards. For example, isolated AC/DC converters are often used to interface storage batteries in uninterruptable power supplies or to transfer energy from photovoltaic panels to the utility power system. The conventional structure for an isolated AC/DC converter generally consists of a front-end power factor correction rectifier, followed by an isolated DC/DC converter. In this structure, an intermediate DC-link is needed to link these two converters and therefore the current from the ac side has to undergo two stages for power transmission.

In order to improve the power density and system efficiency, single-stage AC/DC converters [1], [2] are introduced to replace the conventional two-stage structure. A common approach is to remove the bulky and failure prone DC-link electrolytic capacitors from the converter, which can considerably decrease the weight and volume of the device and also improve the system reliability. However, the converter control will also become more complex compared to the decoupled ac-dc and dc-dc conversion in the conventional two-stage converter.

Considering e.g. the on-board charger in plug-in electric vehicles, bidirectional power flow and electrical isolation between the external ac source and the internal dc battery pack are normally required for smart grid application and also due to safety issues. Because of the high power density and efficiency, dual-active-bridge (DAB) converter is a potential candidate for the single-stage on-board charger design. Many modulation methods have been proposed for the DAB converter, such as the basic single-phase-shift (SPS) modulation [3] and improved methods as described in [4]-[6] to extend the ZVS range or in [7]-[9] to decrease the power degradation. Besides shifting the angles, the switching frequency can also be used as a control variable to improve the DAB light-load performance [10]. However, all these methods are dependent on a constant dc voltage for the input and output of the DAB. In order to incorporate the ac-

dc energy conversion into a single stage, the conventional DAB converter needs to be modified.

In [11], the primary full-bridge in a DAB is replaced by a half bridge, which is comprised of two cascaded capacitors in one leg and four cascaded anti-serial MOSFETs in the other leg, in such a way that the modified converter can transfer energy from ac to dc. Three degrees of freedom are utilized to modulate the converter, including two phase-shift angles and the switching frequency. Based on particular system parameters, pre-calculated control values are determined and stored in a look-up table for the system control. In [12], a similar single-stage ac-dc converter is proposed by replacing each switch in the primary full-bridge of the DAB with two reverse blocking IGBTs. Operating the converter with a fixed switching frequency, the system can achieve open-loop power factor correction (PFC) using only two control variables and realize zero-current switching (ZCS) for the IGBTs. Nonetheless, in [12] only one operation mode is considered, which may not be suitable for higher power transmission. Besides, the ZCS modulation for IGBTs can reduce the switching losses down to a limited extent, if the commonly used MOSFETs are configured for the DAB [13].

Another kind of single-stage DAB ac-dc converter can be seen in [14], which presents a new topology by adding a synchronous rectifier in front of the DAB. Instead of using bidirectional switches, e.g. anti-serial MOSFETs or cascaded reverse blocking IGBTs, the input of DAB has a double-line-frequency (100 Hz/120 Hz) single-polarity voltage after unfolding the rectified grid voltage. With variable switching frequencies, three optimized control variables are pre-calculated and stored in a look-up table such that the DAB can regulate the power factor and achieve ZVS at the same time. The same structure can be found in [15], which uses GaN HEMTs to enhance the efficiency performance.

Due to the complex control of bidirectional switches, this paper focuses on the single-stage ac-dc converter involving a synchronous rectifier. A new control scheme is proposed to extend the achievable power range by adopting two operation modes, and the converter can achieve full-range ZVS during one whole mains cycle for both modes. Besides, the commonly used look-up tables are eliminated, thus the control scheme can be applied to universal single-stage DAB ac-dc converters and not limited by particular system parameters. The structure of this paper is as follows: firstly, the basic principles of two operation modes are presented in section II, then the current regulation principle and ZVS limitations on the control variables are discussed in section III, followed by power range analysis and system control procedure which are shown in section IV. Finally, simulation results and experimental results are illustrated in section V.

## II. BASIC OPERATION

The converter topology shown in Fig. 1 comprises of a front-end synchronous rectifier (SR), converting the sinusoidal ac voltage  $v_{ac}$  into single-polarity positive voltage  $v_2$ , and the rear-end DAB dc-dc converter. A high-frequency transformer is used to link the full bridge HB<sub>1</sub> and HB<sub>2</sub> with a leakage inductance  $L_{tr}$  serving as the energy storage component. In practice, an auxiliary inductor is usually cascaded with the primary winding of the HF transformer, acting as a part of the equivalent leakage inductance. In this paper, the DAB is assumed to work in boost mode, namely

$$V_{ac} < nV_1 \quad (1)$$

where  $n$  is the turns ratio of the transformer,  $V_{ac}$  is the amplitude of the ac voltage and  $V_1$  the dc voltage. Due to that the switches  $G_1 \sim G_4$  in the SR operate at the line frequency ( $f_{ac} = 50 \text{ Hz}/60 \text{ Hz}$ ) and the DAB usually has a much higher switching frequency ( $f_{sw} \gg f_{ac}$ ), the input voltage  $v_2$  is assumed to be constant in one switching period ( $T_{sw} = 1/f_{sw}$ ).

Based on whether the falling edge of the primary voltage  $v_p$  lags or leads that of the secondary voltage  $v_s$ , the typical working waveforms of the DAB are plotted in Fig. 2(a) and Fig. 2(b), which corresponds to Mode I (light load) and Mode II (heavy load), respectively. In the figures,  $\alpha$  represents the duty cycle of  $v_s$  and  $\varphi$  is the phase-shift angle between  $v_p$  and  $v_s$ . Owing to the DAB symmetry and in order to achieve lower inductance current,  $\alpha$  and  $\varphi$  are commonly limited within  $[0, \pi]$  and  $[0, \pi/2]$ , respectively. For simplicity,  $D_\alpha$  and  $D_\varphi$  are introduced as

$$D_\alpha = \frac{\alpha}{\pi} \quad D_\varphi = \frac{\varphi}{\pi} \quad (2)$$

with the range of  $[0, 1]$  and  $[0, 0.5]$ , respectively.

According to the waveforms shown in Fig. 2, the average input current of DAB in one switching period can be derived as

$$I_{2,m1} = \frac{nV_1}{2L_{tr}f_{sw}} D_\varphi D_\alpha \quad (3)$$

$$I_{2,m2} = \frac{nV_1}{8L_{tr}f_{sw}} \left[ 1 - (1 - 2D_\varphi)^2 - (1 - D_\alpha)^2 \right] \quad (4)$$

where  $I_{2,m1}$  and  $I_{2,m2}$  are for Mode I and Mode II, respectively.

On the other hand, in order to achieve ZVS for all DAB switches, the following conditions (5) and (6) should be satisfied for the individual operation mode,

$$\text{Mode I: } i_{p,m1}(t_0) \leq 0, \quad i_{p,m1}(t_1) \geq 0, \quad i_{p,m1}(t_2) \leq 0 \quad (5)$$

$$\text{Mode II: } i_{p,m2}(t_0) \leq 0, \quad i_{p,m2}(t_1) \geq 0, \quad i_{p,m2}(t_2) \geq 0 \quad (6)$$

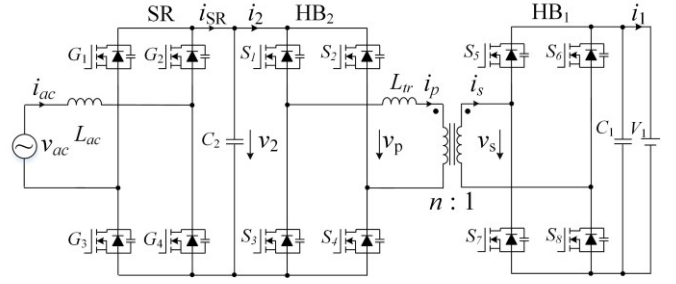


Fig. 1. Dual-active-bridge circuit based bidirectional isolated AC-DC converter with a battery pack load.

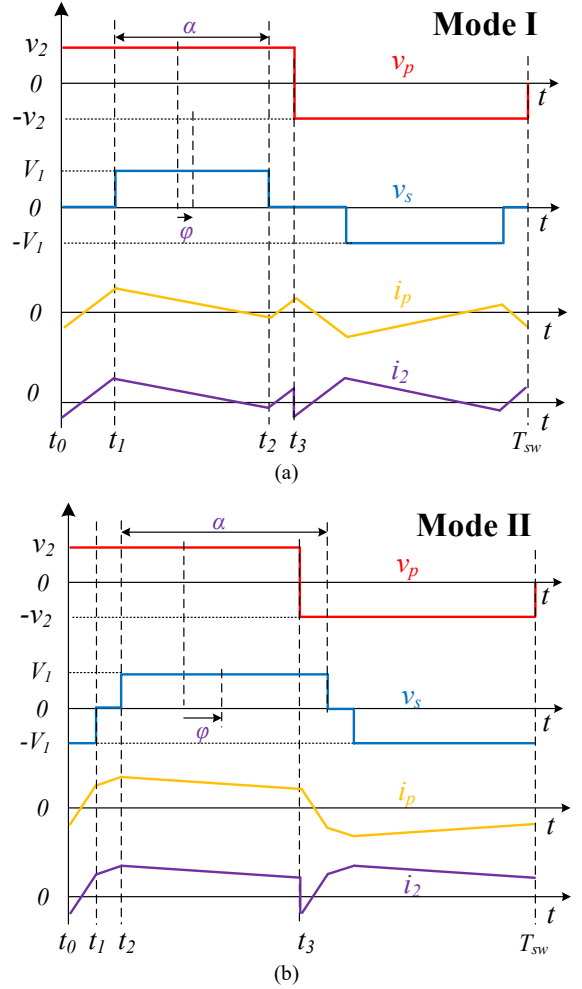


Fig. 2. Typical operating waveforms of the DAB in one switching period: (a) Mode I (light load) (b) Mode II (heavy load)

TABLE I. GENERAL ZVS CONDITIONS FOR DAB CONVERTER

	Mode I	Mode II
Boundary conditions	$0 < D_\alpha \leq 1 - 2D_\varphi$	$1 - 2D_\varphi < D_\alpha \leq 1$
General ZVS constraints	$\frac{2k}{1-k} D_\varphi \leq D_\alpha \leq k$	$\frac{1-k}{2} \leq D_\varphi \leq 0.5$ $\frac{2k(1-D_\varphi)}{1+k} \leq D_\alpha \leq 1$

Thus, the general ZVS conditions for Mode I and Mode II can be obtained, as listed in the second row of Table I. Therein, the symbol  $k$  is defined as  $v_2/nV_1$  with the range of

(0, 1). Besides, the boundary conditions can also be calculated by comparing the falling edge instant of  $v_p$  and  $v_s$  in Fig. 2, and the results are presented in the first row of Table I.

### III. CURRENT CONTROL AND ZVS LIMITATIONS

Over the time range of one mains cycle, the sinusoidal ac voltage and current can be expressed by:

$$v_{ac}(t) = V_{ac} \cdot \sin(2\pi f_{ac}t), \quad i_{ac}(t) = I_{ac} \cdot \sin(2\pi f_{ac}t + \phi) \quad (7)$$

Since the switching frequency of the DAB is much higher than the SR, i.e.  $f_{sw} \gg f_{ac}$ , the ac current  $i_{ac}(t)$  is supposed to be constant during one switching interval of the DAB. Neglecting the current of the high-frequency filtering capacitor  $C_2$ , the instantaneous ac current  $i_{ac}(t)$ , the SR output current  $i_{SR}(t)$  and the DAB average input current  $I_2(t)$  in one switching period are equal to each other.

In addition, for the purpose of achieving unity power factor ( $\phi=0$ ), three control variables  $D_\alpha$ ,  $D_\phi$  and  $f_{sw}$  are employed according to the formulas in Table II.  $C_{m1}$  and  $C_{m2}$  are two coefficients defined as the amplitude of  $D_\alpha$ .

In Mode I, the switching frequency  $f_{sw}$  is fixed at  $f_b$ , which is the base switching frequency of Mode II.  $D_\phi$  and  $D_\alpha$  are used to control the ac current. As Mode II is for higher power transmission,  $D_\phi$  is given as 0.5 to regulate the ac current while the switching frequency  $f_{sw}$  varies within the range of  $[f_b, 2f_b]$ , which is determined by  $D_\alpha$ .

Therefore, the ac current for Mode I and Mode II can be obtained by submitting the expressions of  $D_\alpha$ ,  $D_\phi$  and  $f_{sw}$  into (3) and (4), respectively.

$$i_{ac}(t) = \begin{cases} \frac{nV_1 D_\phi C_{m1}}{2L_{tr} f_b} \cdot |\sin(2\pi f_{ac}t)|, & \text{Mode I} \\ \frac{nV_1 C_{m2}}{8L_{tr} f_b} \cdot |\sin(2\pi f_{ac}t)|, & \text{Mode II} \end{cases} \quad (8)$$

Seen from (8), the amplitude of the ac current is determined by  $D_\phi$  and  $C_{m1}$  when the single-stage DAB AC/DC converter operates in Mode I, and by  $C_{m2}$  in Mode II.

Furthermore, in order to achieve ZVS for all DAB switches over one whole mains cycle, the general ZVS conditions in Table I should be satisfied for any value of  $v_2$ , which is equal to  $V_{ac} \cdot |\sin(2\pi f_{ac}t)|$ . As shown in Fig. 3, the obtained upper and lower limits of  $D_\alpha$  in one mains cycle are plotted with red curves and the yellow areas between them represent the ZVS region. It can be seen that the amplitude of  $D_\alpha$  should be limited in certain ranges for Mode I and Mode II, corresponding to the blue curves in Fig. 3(a) and Fig. 3(b), respectively. Especially, since  $D_\phi$  in Mode I can be utilized to regulate the ac current amplitude according to (8), Fig. 3(c) presents the varying lower limits of  $D_\alpha$  with the change of  $D_\phi$ . Seen from Fig. 3(c), the ZVS range is narrowed down as  $D_\phi$  increases. Based on the expressions of  $D_\alpha$  and  $D_\phi$  in Table II, the ZVS conditions for the single-stage DAB AC/DC converter can be derived, as presented in the last row of Table II.

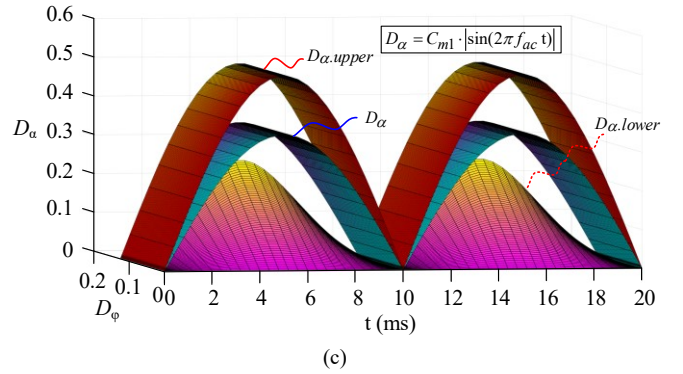
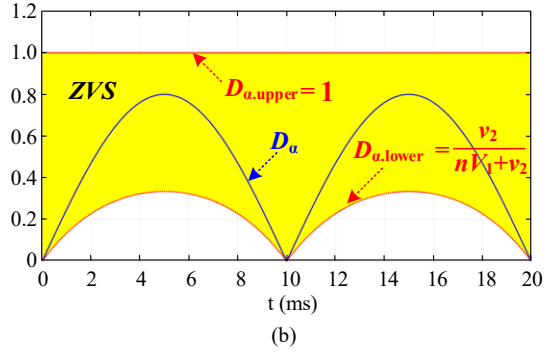
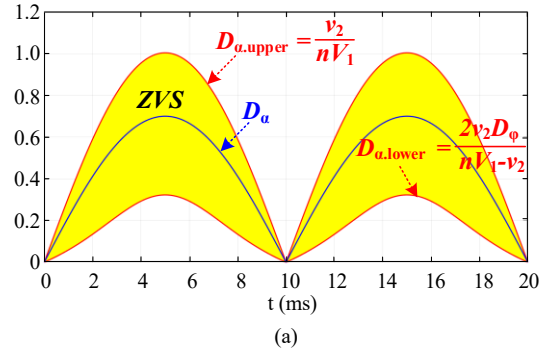


Fig. 3. ZVS range during one mains cycle: (a) Mode I with a specific  $D_\phi$  (b) Mode II (c) Mode I with varying  $D_\phi$

TABLE II. EXPRESSIONS OF CONTROL VARIABLES AND ZVS CONDITIONS FOR SINGLE-STAGE DAB AC/DC CONVERTER

	Mode I	Mode II
$D_\phi$	$0 < D_\phi \leq \frac{nV_1 - V_{ac}}{2nV_1}$	0.5
$D_\alpha$	$C_{m1} \cdot  \sin(2\pi f_{ac}t) $	$C_{m2} \cdot  \sin(2\pi f_{ac}t) $
$f_{sw}$	$f_b$	$f_b \cdot (2 - D_\alpha)$
ZVS conditions	$\frac{2V_{ac}D_\phi}{nV_1 - V_{ac}} \leq C_{m1} \leq \frac{V_{ac}}{nV_1}$	$\frac{V_{ac}}{nV_1} \leq C_{m2} \leq 1$

### IV. POWER RANGE AND SYSTEM CONTROL

In one switching period, the average transmitted power to the DAB for Mode I and Mode II can be calculated from Fig. 2, and according to Table II, the range of instantaneous power can be deduced as:

$$[P_{m1.min}, P_{m1.max}] = \left[ 0, \frac{2V_{ac}^2 \cdot (nV_1 - V_{ac})}{(nV_1)^3} \cdot |\sin(2\pi f_{ac}t)|^2 \right] \quad (9)$$

$$[P_{m2.min}, P_{m2.max}] = \left[ \frac{V_{ac}^2 \cdot |\sin(2\pi f_{ac}t)|^2}{nV_1(nV_1 + V_{ac})}, \frac{V_{ac}}{nV_1} \cdot |\sin(2\pi f_{ac}t)|^2 \right] \quad (10)$$

Note that a base value of  $(nV_1)^2/8L_{\text{tf}}f_b$  is employed for the power calculation. Limited by the ZVS conditions,  $P_{m1.min}$  and  $P_{m1.max}$  are the achievable minimum and maximum power transfer in Mode I, respectively, while  $P_{m2.min}$  and  $P_{m2.max}$  are power transfer with mode II. The boundary condition for  $P_{m1.max}$  equaling  $P_{m2.min}$  is:

$$\frac{V_{ac}}{nV_1} = \frac{1}{\sqrt{2}} \quad (11)$$

In terms of system control, the operation mode can be selected according to (9), (10) and (11). If  $V_{ac}/nV_1$  is higher than  $1/\sqrt{2}$ , leading to  $P_{m1.max} < P_{m2.min}$ , Mode I and Mode II would have an independent power range. As shown in Fig. 4(a), the dark and light grey areas are the power ranges of Mode I and Mode II, respectively. Considering the maximum value of the output power, the converter will work in Mode I if the maximum needed power is lower than  $2V_{ac}^2(nV_1 - V_{ac})/(nV_1)^3$  or Mode II if it is larger than  $V_{ac}^2/[nV_1 \cdot (nV_1 + V_{ac})]$ .

For the situation when  $V_{ac}/nV_1$  is lower than  $1/\sqrt{2}$ , the power range of Mode I and Mode II would have an overlapped area, as presented in Fig. 4(b). If the maximum output power is located within this area, the DAB is set to work in Mode I in order to avoid variable switching frequency, which may have an adverse effect on other system performances like the electromagnetic interference.

The system control process is illustrated in Fig. 5. The voltage and current on the ac side ( $v_{ac}$ ,  $i_{ac}$ ) are sampled to calculate the grid phase angle  $\theta_{ac}$  and the actual d-axis current component  $i_d$ . Here the sliding discrete transform-based phase-locked loops (SDFT-PLL) is adopted to accurately obtain the actual amplitude of the ac current because of its advantages of fast dynamic response and good harmonic filtering performance over other PLL methods [16]. Assuming that the ac grid is ideal, the basic derivative phase-locked loop (DPLL) is chosen for the phase-angle lock, because of its low computational burden.

Next, the error between the reference current amplitude and actual value is used to generate the coefficient  $C_m$ , which is used as  $C_{m1}$  for Mode I or  $C_{m2}$  for Mode II, depending on the aforementioned mode selection result. Here, the reference ac current amplitude  $I_{ac}^*$  can be calculated using the needed input ac charging power and the grid voltage. Based on  $C_m$ ,  $\theta_{ac}$  and the expressions in Table II, the values of  $D_\phi$ ,  $D_\alpha$  and  $f_s$  can be achieved. Together with the positive or negative ac voltage, the switching signals for the single-stage isolated AC/DC converter system can be obtained.

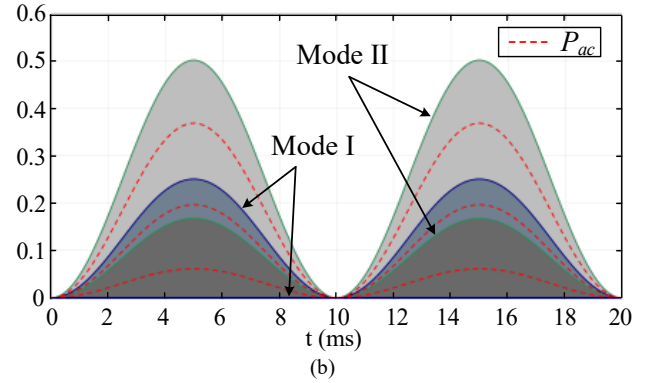
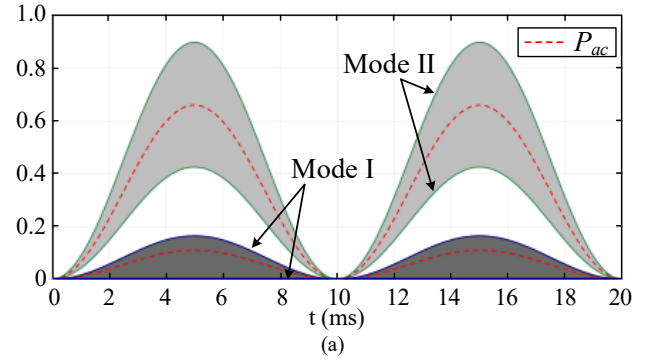


Fig. 4. Power ranges of Mode I and Mode II over an ac mains cycle when: (a)  $V_{ac}/nV_1 < 1/\sqrt{2}$  and (b)  $V_{ac}/nV_1 > 1/\sqrt{2}$ .

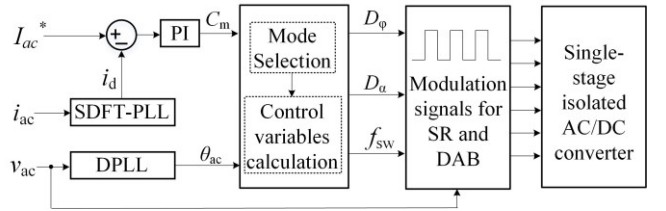


Fig. 5. System control block for the single-stage DAB ac-dc converter

TABLE III. COMPONENT PARAMETERS FOR EXPERIMENTAL SETUP

Components	Parameters
MOSFETs $G_1 \sim G_4, S_1 \sim S_4$ (IPW65R080CFD)	$R_{ds,onp} = 14.4 \text{ m}\Omega$
MOSFETs $S_5 \sim S_8$ (IPP110N20N3)	$R_{ds,ons} = 1.9 \text{ m}\Omega$
HF transformer winding resistance	Primary $R_{tr,p} = 121.6 \text{ m}\Omega$ Secondary $R_{tr,s} = 3.3 \text{ m}\Omega$
HF transformer magnetic core (TDK ETD59 ferrite core)	$K_m = 0.0717, f = f_s, \beta = 1.72,$ $\gamma = 2.66, B = 0.32 \text{ T}, V_{tr} = 51.2 \text{ cm}^3$
Auxiliary inductor (ER42)	$R_{aux} = 5.6 \text{ m}\Omega$

## V. SIMULATION AND EXPERIMENT

For the single-stage DAB ac-dc converter design, Table III summarizes the selected circuit components and related parameters. In the secondary HB<sub>1</sub> of DAB, each switch is composed of two paralleled MOSFETs to increase the current tolerance and reduce the switching losses. As it is shown in Fig. 6, the single DAB prototype is configured with the components listed in Table III.

TABLE IV. CONVERTER PARAMETERS

Parameters	Values
AC voltage (rms)	85 V
HF filter inductance $L_{ac}$	200 $\mu$ H
HF filter capacitor $C_2$	20 $\mu$ F
Base switching frequency $f_b$	25 kHz
DC voltage $V_1$	70 V
Turns ratios $n : 1$	3.5 : 1
Leakage inductance $L_{tr}$	45 $\mu$ H
Dead time $T_{dead}$	200 ns

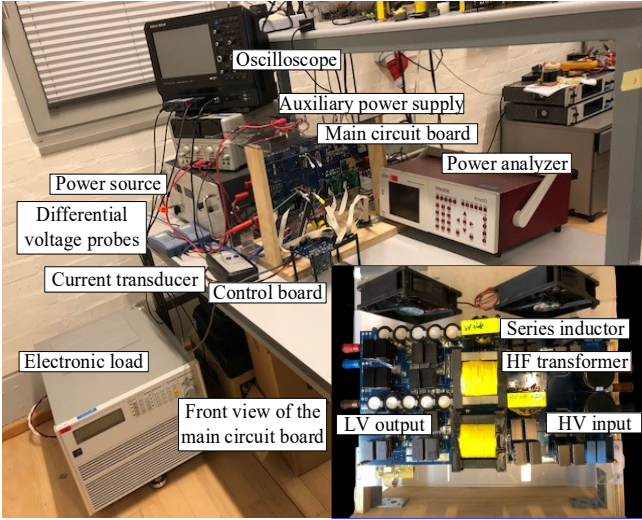


Fig. 6. Test platform for the single DAB dc-dc converter.

Using the converter parameters listed in Table IV, the simulated working waveforms of the converter are shown in Fig. 7. At the instant of 0.08 s, the transmission power of the converter is boosted from 270 W to 1500 W. The ac voltage  $v_{ac}$  and ac current  $i_{ac}$  are displayed in Fig. 7(a). The measured total harmonic distortion (THDi) of the ac current is also marked in the figure, both of which are below 5%. Besides, seen from the waveforms of  $i_p$  shown in Fig. 7(c) and Fig. 7(d), the converter switches from the operation Mode I to Mode II accordingly, which indicates a seamless mode transfer depending on the different power requirements.

Besides, in order to observe the power transition in the high-frequency DAB converter, the waveforms of the primary voltage  $v_p$ , the secondary voltage  $v_s$  and the leakage inductor current  $i_p$  are illustrated in Fig. 7(b). Seen from the envelopes of  $i_p$ , the current increases to a higher level at the time of 0.08 s to transmit higher power. Meanwhile, the primary and secondary voltage are unchanged due to a stable ac voltage and load-side dc voltage.

Furthermore, in order to judge whether the switches in the DAB have realized ZVS, waveforms of the near-zero voltage area of Mode I and Mode II are amplified, as shown in Fig. 7(c) and Fig. 7(d), respectively. Seen from the dashed lines, the rising and falling edges of  $v_p$  corresponds

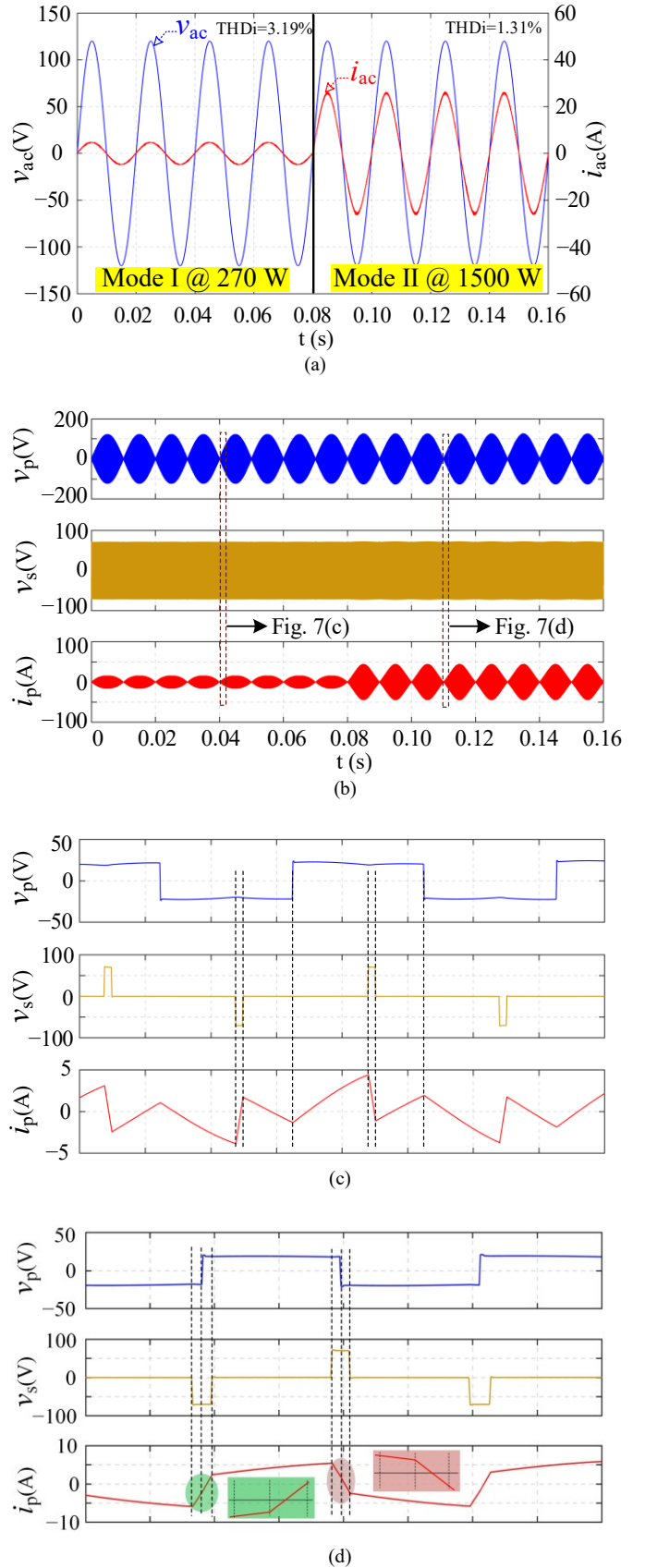


Fig. 7. Operating waveforms of the single-stage DAB AC/DC converter where the given transmitted power is changed from 270 W to 1500 W : (a) ac-side voltage  $v_{ac}$  and current  $i_{ac}$  with measured THD (b) the primary voltage  $v_p$ , secondary voltage  $v_s$  and the leakage inductor current  $i_p$  in DAB stage (c) zoom-in waveforms of the near-zero area in Mode I (d) zoom-in waveforms of the near-zero area in Mode II.

to negative and positive leakage inductance current, respectively, which indicates ZVS of the primary four switches. On the contrary, at the instants of rising and falling edges of  $v_s$ , the leakage current is positive or negative, leading to ZVS of the secondary four switches. In general, ZVS is relatively more difficult to achieve when the DAB works in light-load conditions, corresponding to the near-zero ac voltage area in Fig. 7(b). Thus, it can be concluded that all DAB switches can realize zero-voltage switching for both operation modes during one whole mains cycle.

In addition, an experimental platform to evaluate the single DAB converter is built, as illustrated in Fig. 6. Obtained experimental results are shown in Fig. 8(a) and Fig. 8(b), corresponding to Mode I and Mode II, respectively. Noting that the experimental waveforms are measured from a single DAB dc-dc converter to emulate the operating points in one switching interval, during which the ac voltage is unchanged. The input and output dc voltages are respectively 120 V and 70 V, which are equal to the simulated peak ac voltage and dc-side voltage of the single-stage ac-dc converter. The switching frequencies of Mode I and Mode II are set to be 25 kHz and 50 kHz, which are the same as the simulated switching frequency in Mode I and the maximum switching frequency in Mode II. Similar to the simulation results, the dual-active-bridge dc-dc converter is able to achieve zero-voltage switching when the single DAB works at 400 W in Mode I or 980 W in Mode II.

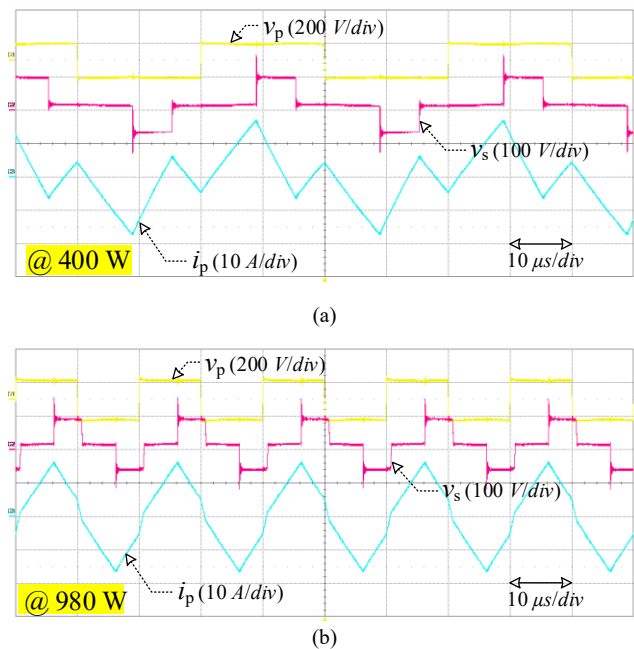


Fig. 8. Test waveforms for the single DAB dc-dc converter (a) Mode I (b) Mode II.

## VI. CONCLUSION

In this paper, a flexible control scheme for the single-stage DAB based ac-dc converter is proposed. The converter can work in two operation modes and switch between them flexibly so that the converter power range can be extended. Besides, the control scheme can achieve unity power factor and zero-voltage switching over one full mains cycle without using look-up tables. The theoretical analysis is

validated by simulation results and furthermore, some experimental waveforms are also shown.

## REFERENCES

- [1] B. Singh, B. N. Singh, A. Chandra, K. Al-Haddad, A. Pandey, and D. P. Kothari, "A review of single-phase improved power quality AC-DC converters," *IEEE Trans. on Industrial Electronics*, vol. 50, no. 5, pp. 962–981, 2003.
- [2] J. P. M. Figueiredo, F. L. Tofoli, and B. L. A. Silva, "A review of single-phase PFC topologies based on the boost converter," in *proc. of IEEE/IAS International Conference on Industry Applications*, 2010, pp. 1–6.
- [3] J. Everts, J. Van den Keybus, F. Krismer, J. Driesen, and J. W. Kolar, "Switching control strategy for full ZVS soft-switching operation of a dual active bridge AC/DC Converter," in *proc. of IEEE 27th Annual IEEE Applied Power Electronics Conference and Exposition*, 2012, pp. 1048-1055.
- [4] H. Zhou and A. M. Khambadkone, "Hybrid modulation for dual-active bridge bidirectional converter with extended power range for ultracapacitor application," *IEEE Trans. on Industry Applications*, vol. 45, no. 4, pp. 1434-1442, Jul.-Aug. 2009.
- [5] A. K. Jain and R. Ayyanar, "PWM control of dual active bridge: Comprehensive analysis and experimental verification," *IEEE Trans. on Power Electronics*, vol. 26, no. 4, pp. 1215-1227, Apr. 2011.
- [6] G. G. Oggier and M. Ordonez, "High efficiency DAB converter using switching sequences and burst-mode," *IEEE Trans. on Power Electronics*, vol. 31, no. 3, pp. 2069-2082, Mar. 2016.
- [7] G. Oggier, G. O. Garcí and A. R. Oliva, "Modulation strategy to operate the dual active bridge DC-DC converter under soft switching in the whole operating range," *IEEE Trans. on Power Electronics*, vol. 26, no. 4, pp. 1228-1236, Apr. 2011.
- [8] G. R. C. Mouli, J. H. Schjffelen, P. Bauer, and M. Zeman, "Design and Comparison of a 10-kW Interleaved Boost Converter for PV Application Using Si and SiC Devices," *IEEE Journal of Emerging and Selected Topics in Power Electronics*, vol. 5, no. 2, pp. 610-623, Jun. 2017.
- [9] B. Liu, P. Davari and F. Blaabjerg, "An Optimized Control Scheme for Reducing Conduction and Switching Losses in Dual Active Bridge Converters," in *proc. of IEEE Energy Conversion Congress and Exposition*, 2018, in press.
- [10] G. Guidi, M. Pavlovsky, A. Kawamura, T. Imakubo, and Y. Sasaki, "Improvement of light load efficiency of dual active bridge DC-DC converter by using dual leakage transformer and variable frequency," in *proc. of IEEE Energy Conversion Congress and Exposition*, 2010, pp. 830–837.
- [11] F. Jauch and J. Biela, "Combined Phase-Shift and Frequency Modulation of a Dual-Active-Bridge AC-DC Converter With PFC," *IEEE Trans. on Power Electronics*, vol. 31, no. 12, pp. 8387 – 8397, 2016.
- [12] N. D. Weise, G. Castelino, K. Basu and N. Mohan, "A Single-Stage Dual-Active-Bridge-Based Soft Switched AC-DC Converter With Open-Loop Power Factor Correction and Other Advanced Features," *IEEE Trans. on Power Electronics*, vol. 29, no. 8, pp. 4007 - 4016, 2014.
- [13] R. W. Erickson and D. Maksimovic, *Fundamentals of Power Electronics*. Springer Science & Business Media, 2001.
- [14] J. Everts, F. Krismer, J. V. Keybus, J. Driesen, and J. W. Kolar, "Optimal ZVS Modulation of Single-Phase Single-Stage Bidirectional DAB AC-DC Converters," *IEEE Trans. on Power Electronics*, vol. 29, no. 8, pp. 3954 - 3970, 2014.
- [15] J. Lu, Q. Tian, K. Bai, A. Brown, and M. McAmmond, "An indirect matrix converter based 97%-efficiency on-board level 2 battery charger using E-mode GaN HEMTs," in *proc. of IEEE 3rd Workshop on Wide Bandgap Power Devices and Applications*, 2015, pp. 351 – 358.
- [16] S. Golestan, J. M. Guerrero and J. C. Vasquez, "Single-Phase PLLs: A Review of Recent Advances," *IEEE Trans. on Power Electronics*, vol. 32, no. 12, pp. 9013 - 9030, 2017.